PASJ: Publ. Astron. Soc. Japan **64**, 75, 2012 August 25

Grand Rotation Curve and Dark-Matter Halo in the Milky Way Galaxy

Yoshiaki SOFUE
Department of Physics, Meisei University, Hino-shi, Tokyo 191-8506
Institute of Astronomy, The University of Tokyo, Mitaka, Tokyo 181-0015
sofue@ioa.s.u-tokyo.ac.jp

(Received 2011 August 22; accepted 2012 January 19)

Abstract

A grand rotation curve of the Milky Way Galaxy was constructed, which covers a wide range of radius from the Galactic Center to ~ 1 Mpc, and was deconvolved into bulge, disk, and halo components by least-squares fittings. We determined the masses and scale radii of the bulge and disk to be $M_{\rm b} = (1.652 \pm 0.083) \times 10^{10}\,M_\odot$, $a_{\rm b} = 0.522 \pm 0.037$ kpc, $M_{\rm d} = (3.41 \pm 0.41) \times 10^{10}\,M_\odot$, and $a_{\rm d} = 3.19 \pm 0.35$ kpc. The dark halo was fitted by the Navaro–Frenk–White (NFW) density profile, $\rho = \rho_0/[(R/h)(1 + R/h)^2]$, and the fit yielded $h = 12.5 \pm 0.9$ kpc and $\rho_0 = (1.06 \pm 0.14) \times 10^{-2}\,M_\odot\,{\rm pc}^{-3}$. The local dark-matter density near the Sun at $R_0 = 8$ kpc was estimated to be $\rho_0^\odot = (6.12 \pm 0.80) \times 10^{-3}\,M_\odot\,{\rm pc}^{-3} = 0.235 \pm 0.030\,{\rm GeV\,cm}^{-3}$. The total mass inside the gravitational boundary of the Galaxy at $R \sim 385$ kpc, a half distance to M 31, was estimated to be $M_{\rm b+d+h} = (7.03 \pm 1.01) \times 10^{11}\,M_\odot$. This leads to a stellar baryon fraction of $M_{\rm b+d}/M_{\rm b+d+h} = 0.072 \pm 0.018$. Considering the expected baryon fraction in the Local Group, we suggest that baryons in the form of hot gas are filling the dark halo with a temperature of $\sim 10^6$ K and an emission measure of $\sim 10^{-5}\,{\rm pc\,cm}^2$. Such hot halo gas may share a small fraction of the observed X-ray background emission.

Key words: Galaxy: fundamental parameters — Galaxy: rotation curve — Galaxy: structure — galaxies: dark matter

1. Introduction

The dynamical mass distribution in the Milky Way Galaxy is principally determined by analyzing the rotation curve on the assumption of circular rotation of the Galactic disk (e.g., Sofue & Rubin 2001). In our previous work, a large-scale rotation curve, called pseudo-rotation curve, was obtained by combining the current rotation curve and the radial velocities of globular clusters and satellite galaxies, which was used to model the Galaxy's mass components (Sofue, et al. 2009, Paper I; Sofue 2009, Paper II). While the fitting to the inner rotation curves was satisfactory, the outermost mass structure related to the dark halo was still crude because of the large scatter of the used kinematical data. It has been shown that the kinematics of satellite galaxies is crucial for determining the global dark halo models.

In this paper we constructed a new large-scale, running averaged rotation curve, which we call the grand rotation curve. We analyzed it more quantitatively and accurately compared to the previous work using the least-squares fitting method. We adopted the de Vaucouleurs (1958) profile for the bulge, exponential disk (Freeman 1970), and NFW (Navaro et al. 1996) density profile for the dark halo.

Throughout the present work, we adopted a galacto-centric distance and circular velocity of the Sun of $(R_0, V_0) = (8.0\,{\rm kpc}, 200\,{\rm km\,s}^{-1})$. The result of the local dark-matter density will be compared with the most recent values from extensive analyses of the Galactic rotation curve (Xue et al. 2008; Weber & de Boer 2010; Salucci et al. 2010). The fitted parameters for the bulge, disk, and dark halo will be used to estimate the baryon fraction inside the supposed Galaxy boundary at ~ 385 kpc, a half distance to M 31. The estimated emission measure of hot gas will be compared with the observed X-ray background.

2. Observed Rotation Curve and Velocity Dispersion

Figure 1 shows the observed rotation velocities, $V(R)$, and the galacto-centric radial velocities, $V_{\rm GC:obs}$, as reproduced from Papers I and II, where we compiled kinematical data from the literature and recalculated them for Galactic constants of $(R_0, V_0) = (8\,{\rm kpc}, 200\,{\rm km\,s}^{-1})$. The inner data within $R \sim 10$ kpc are mostly from traditional circular velocity measurements of disk objects near the Galactic plane, while some data with large scatter are the galacto-centric velocities of globular clusters. The data from 10 to $\sim$25 kpc are a mixture of usual circular velocities and galacto-centric radial velocities of globular clusters. Those beyond $R \sim 30$ kpc are $V_{\rm GC:obs}$ of distant globular clusters, satellite galaxies, dwarf galaxies, and member galaxies of the Local Group. See Paper II for details and data references. We included the circular velocities from an SDSS blue stars analysis by Xue et al. (2008; their model 1) by correcting for a systematic difference in the velocities of about $-20\,{\rm km\,s}^{-1}$, due to our $V_0 = 200\,{\rm km\,s}^{-1}$ instead of their $220\,{\rm km\,s}^{-1}$. We also added recent accurate rotation velocities from VERA for stellar maser sources (Honma et al. 2007; Oh et al. 2010).

A rotation curve is defined by the circular velocity, $V_{\rm circ}$, in a balance between the centrifugal force and gravity, which is equivalent to the virial theorem of circularly rotating disk objects. For non-disk objects, like globular clusters and satellites that are moving in statistical and/or random orbits in virial

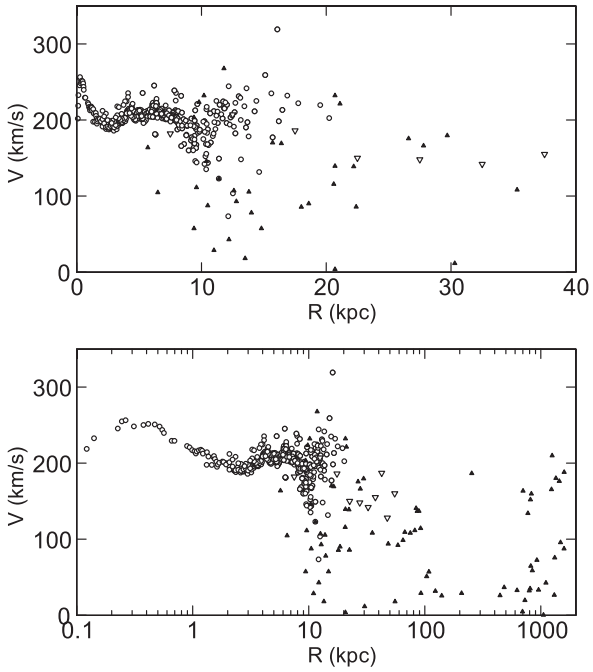

Fig. 1. (Top) Rotation velocities and galacto-centric radial velocities made from the data list in Paper II. Circles are disk objects, triangles are non-disk objects showing their galacto-centric radial velocities (not multiplied by $\sqrt{2}$), and reverse triangles are circular velocities from Xue et al. (2008). (Bottom) Same, but in logarithmic scaling up to 1 Mpc.

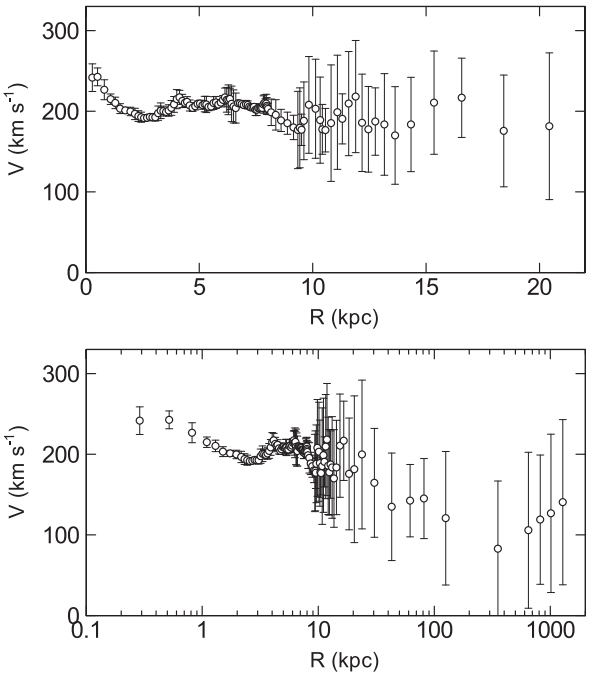

Fig. 2. Rotation curve, $V(R_i)$, of the Galaxy obtained by a running mean of $11 = 2 \times 5 + 1$ neighboring data at every 5 data points in the order of increasing radius. The bars indicate the least-squares fit dispersion in each bin. The top panel shows the data within 25 kpc, and the bottom within the Local Group. Note the abscissa in the bottom figure is logarithmic.

equilibrium, we define a pseudo-rotation velocity as galacto-centric velocity, $V_{\rm GC}$, corrected for the freedom of motion of individual objects; it is related to the observed galacto-centric velocity as $V_{\rm GC} = \sqrt{2}\, V_{\rm GC:obs}$, where $\sqrt{2}$ is a correction factor for possible tangential motion of the object, as expected from its observed radial velocity. We thus define the rotation curve as

$$W(R) = V_{\rm circ} \tag{1}$$

for disk objects (H I gas, CO gas, molecular clouds, H II regions, OB stars, and red giants in the disk), and

$$W(R) = V_{\rm GC} = \sqrt{2} V_{\rm GC:obs} \tag{2}$$

for non-disk objects (globular clusters, satellites, dwarf galaxies, Local Group galaxies).

In order to obtain a smooth rotation curve, we apply a running mean of the observed values in figure 1. We define the rotation velocity at R_i as

$$V(R_i) = \frac{\Sigma_{j=i-N}^{i+N} W(R_j)}{2N+1}, \tag{3}$$

where $2N + 1$ is the number of used data points around $R = R_i$, which is taken every N steps in the data list in the order of increasing radius. In the present paper we take $N = 5$, so that the data are running averaged every $N = 5$ points using their neighboring $2N + 1 = 11$ objects. We also calculate the velocity dispersion by

$$\sigma(R_i) = \sqrt{\frac{\Sigma_{j=i-N}^{i+N} [V(R_j) - W(R_i)]^2}{(2N+1)-1}}. \tag{4}$$

Figure 2 shows the obtained rotation curve, and table 1 lists the values. Note that the observational errors of individual data points are much less than the scatter in this plot, i.e., $\sigma(R_i)$ is much larger than the observational error. In this meaning, $\sigma(R_i)$ represents the real velocity dispersion of the objects in each averaging bin. A table of the obtained rotation velocities used for figure 2 (table 1) is available from our URL.[1]

3. The Models

We assume that the rotation curve is composed of a bulge, disk, and dark halo components, and is calculated by

$$V(R)^2 = V_{\rm b}(R)^2 + V_{\rm d}(R)^2 + V_{\rm h}(R)^2, \tag{5}$$

where $V(R)$, $V_{\rm b}(R)$, $V_{\rm d}(R)$, and $V_{\rm h}(R)$ are the circular rotation velocity at the galacto-centric distance R, the corresponding circular velocity due to the bulge, disk, and dark halo, respectively. Using the newly constructed rotation curve in figure 2, we construct a model rotation curve using the least-squares fitting.

3.1. Bulge

The bulge is assumed to have the de Vaucouleurs (1958) profile for the surface mass density as

[1] ⟨http://www.ioa.s.u-tokyo.ac.jp/∼sofue/htdocs/2012DarkHalo/⟩.

Table 1. Grand rotation curve of the Galaxy.*

Radius (kpc)	Velocity ($km\,s^{-1}$)	Velo. dispersion ($km\,s^{-1}$)	Radius (kpc)	Velocity ($km\,s^{-1}$)	Velo. dispersion ($km\,s^{-1}$)	Radius (kpc)	Velocity ($km\,s^{-1}$)	Velo. dispersion ($km\,s^{-1}$)
0.29	241.68	17.15	5.63	210.14	7.93	8.88	185.18	13.73
0.52	242.67	11.06	5.74	210.94	7.41	9.16	179.90	15.12
0.82	226.67	12.34	5.84	208.27	2.84	9.35	176.79	47.92
1.10	214.93	6.44	5.95	210.60	3.97	9.43	179.48	49.56
1.30	210.32	7.12	6.05	214.04	5.47	9.51	177.00	19.42
1.51	203.26	6.14	6.13	217.10	11.67	9.61	188.14	48.17
1.74	201.01	3.76	6.21	214.21	15.33	9.84	207.90	59.99
1.97	199.71	5.23	6.28	214.19	18.46	10.13	203.08	61.44
2.17	196.65	7.07	6.35	215.27	13.26	10.33	189.00	53.36
2.32	193.97	6.63	6.42	209.18	21.97	10.43	177.57	30.87
2.44	192.61	6.22	6.51	205.94	20.53	10.56	176.56	26.96
2.57	191.40	4.05	6.61	203.96	18.62	10.81	185.25	72.22
2.70	191.84	3.76	6.71	209.96	1.64	11.09	198.74	70.78
2.82	192.93	3.29	6.79	209.73	3.30	11.31	190.52	31.04
2.94	192.51	3.70	6.87	208.78	3.44	11.59	209.52	64.58
3.06	192.54	4.76	6.96	207.64	2.83	11.89	218.16	69.56
3.19	197.59	8.86	7.06	208.47	4.98	12.18	185.67	60.42
3.30	200.61	9.73	7.14	207.87	4.96	12.46	177.61	53.11
3.42	200.16	6.08	7.21	205.69	2.87	12.76	187.25	41.79
3.54	199.11	3.43	7.28	204.68	2.82	13.16	183.61	63.00
3.65	200.92	7.10	7.35	205.02	3.67	13.63	169.95	60.50
3.77	204.13	9.23	7.41	205.48	3.38	14.33	183.58	58.46
3.89	208.48	9.79	7.48	202.02	7.30	15.35	210.68	64.01
4.01	215.06	11.90	7.54	201.82	7.20	16.57	216.70	49.18
4.13	217.24	8.67	7.60	203.75	2.28	18.43	175.61	69.31
4.25	212.75	8.18	7.66	203.36	3.02	20.43	181.42	91.02
4.36	210.44	4.87	7.72	203.73	3.58	23.81	199.71	92.24
4.47	211.66	6.42	7.78	204.03	3.10	30.42	164.53	67.49
4.58	207.17	6.82	7.83	208.38	10.80	42.97	134.85	66.69
4.70	204.11	4.28	7.87	210.16	10.21	61.88	142.41	44.90
4.82	206.15	4.52	7.92	208.39	7.09	81.39	145.05	49.65
4.93	209.06	3.71	7.95	209.52	11.52	125.49	120.67	82.77
5.04	209.52	4.25	7.98	206.54	10.40	353.29	82.83	83.95
5.15	207.54	5.06	7.99	204.74	4.87	647.55	105.77	96.74
5.24	208.90	9.63	8.04	202.92	7.16	817.71	118.92	80.17
5.32	208.38	10.02	8.17	198.71	16.40	1012.54	126.69	98.22
5.41	205.36	4.74	8.38	195.51	18.80	1279.93	140.53	102.43
5.52	205.82	4.40	8.61	188.61	13.70			

* The data are running-averaged values using the compiled data in Papers I and II (Sofue et al. 2009; Sofue 2009), data from VERA (Honma et al. 2007; Oh et al 2010), and those from Xue et al. (2008). Ascii data for this table is available from URL ⟨http://www.ioa.s.u-tokyo.ac.jp/∼sofue/htdocs/2012DarkHalo/⟩. Note that, in order to avoid unnecessary smoothing of the steeply varying curve around the bulge component, the fitting was obtained by replacing the data in the table at $R < 2$ kpc with the denser original data points (before running average).

$$\Sigma_{\rm b}(r) = \Sigma_{\rm be} \exp\left\{-\kappa\left[\left(\frac{r}{a_{\rm b}}\right)^{1/4} - 1\right]\right\}, \tag{6}$$

where $\kappa = 7.6695$; $\Sigma_{\rm be}$ is the surface mass density at the scale radius $R = a_{\rm b}$. Note that the scale radius, $a_{\rm b}$, is defined so that the enclosed mass (luminosity) within the cylinder of radius $a_{\rm b}$ is equal to half of the total mass (luminosity). The total mass is calculated by

$$M_{\rm b} = 2\pi \int_0^\infty r\Sigma_{\rm b}(r) dr = \eta {a_{\rm b}}^2 \Sigma_{\rm be}, \tag{7}$$

with $\eta = 22.665$ being a dimensionless constant (Paper I for detail). The mass within a sphere of radius R is given by

$$M_{\rm b}(R) = 4\pi \int_0^R \rho_{\rm b}(r) r^2 dr, \tag{8}$$

where the volume density is calculated using $\Sigma_{\rm b}$ as

$$\rho_{\rm b}(r) = \frac{1}{\pi} \int_r^\infty \frac{d\Sigma_{\rm b}(x)}{dx} \frac{1}{\sqrt{x^2 - r^2}} dx. \tag{9}$$

The circular rotation velocity is then given by

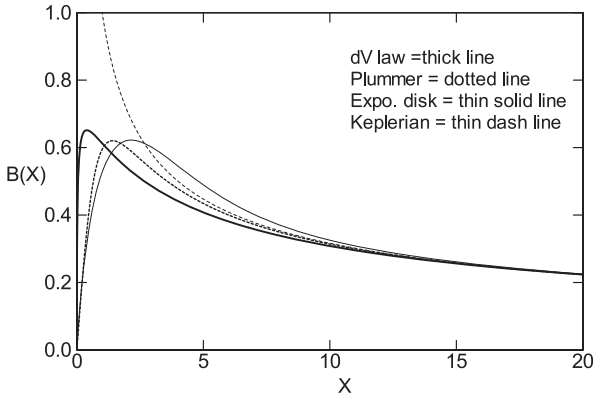

Fig. 3. $\mathscr{B}(X)$ function plotted against $X = R/a_{\rm b}$. For a comparison, we show the Plummer potential, flat exponential disk $\mathscr{D}(X)$ function with $X = R/a_{\rm d}$, and Keplerian law.

$$V_{\rm b}(R) = \sqrt{\frac{GM_{\rm b}}{a_{\rm b}}}\mathscr{B}(X), \tag{10}$$

where $X = R/a_{\rm b}$, and

$$\mathscr{B}(X) = \left[\frac{1}{X}\int_0^X y^2 \int_y^\infty \frac{\frac{d}{dx}e^{-\kappa(x^{1/4}-1)}}{\sqrt{x^2-1}}dxdy\right]^{1/2}. \tag{11}$$

In the fitting procedure, $M_{\rm b}$ and $a_{\rm b}$ are taken as the two free parameters. The time-consuming integral in the above equation was computed by calling a function subroutine that refers to a prepared table of $\mathscr{B}(X)$. Figure 3 shows the $\mathscr{B}$ function as compared with the other useful laws corresponding to the unity total mass and unity scale length. Obviously, all laws tend to be the Keplerian law at sufficiently large radii.

3.2. Disk

The Galactic disk is approximated by an exponential disk, whose surface mass density is expressed as

$$\Sigma_{\rm d}(R) = \Sigma_0 \exp\left(-\frac{R}{a_{\rm d}}\right), \tag{12}$$

where Σ_0 is the central value and $a_{\rm d}$ is the scale radius. The total mass of the exponential disk is given by

$$M_{\rm d} = \int_0^\infty 2\pi r \Sigma_{\rm d} dr = 2\pi \Sigma_0 {a_{\rm d}}^2. \tag{13}$$

The rotation curve for a thin exponential disk is expressed by

$$V_{\rm d}(R) = \sqrt{\frac{GM_{\rm d}}{a_{\rm d}}}\mathscr{D}(X), \tag{14}$$

where $X = R/a_{\rm d}$, and

$$\mathscr{D}(X) = (X/\sqrt{2}) \times [I_0(X/2)\,K_0(X/2) - I_1(X/2)\,K_1(X/2)]^{1/2} \tag{15}$$

with I_i and K_i being modified Bessel functions (Freeman 1970). As the two free parameters, we chose the total mass, $M_{\rm d}$, and scale radius, $a_{\rm d}$.

3.3. Dark Halo

For the dark halo, three mass models have so far been proposed: the semi-isothermal spherical distribution (Begeman et al. 1991), NFW (Navarro et al. 1996), and Burkert (1995) models. In Paper II, we have shown that the isothermal model may not be a good approximation to the observed rotation curve, and showed that the NFW and Burkert models may better fit the observations.

Since the NFW and Burkert profiles are essentially the same, except for the very inner region where the contribution from the dark halo component is negligible, we here adopt the NFW profile. It is expressed as

$$\rho(R) = \frac{\rho_0}{X\,(1+X)^2}, \tag{16}$$

where $X = R/h$, and ρ_0 and h are the representative (scale) density and radius (core radius) of the dark halo, respectively.

The enclosed mass within a radius R is given by

$$M_{\rm h}(R) = 4\pi\rho_0 h^3 \left[\ln(1+X) - \frac{X}{1+X}\right]. \tag{17}$$

The mass enclosed within a radius h is given by ${M_{\rm h}}^* = 2.4272\,\rho_0 h^3$ for $X = 1$, which we call the scaling mass of the dark halo.

The circular rotation velocity at a given distance R is given by

$$V_{\rm h}(R) = \sqrt{\frac{GM_{\rm h}(R)}{R}}. \tag{18}$$

In the fitting procedure, we chose ρ_0 and h as the two free parameters.

4. Fitting Procedure

We search for the best-fit parameters for the bulge, disk, and dark halo using the least-squares method. The free parameters are $M_{\rm b}$, $a_{\rm b}$, $M_{\rm d}$, $a_{\rm d}$, ρ_0, and h.

4.1. Data

We divided the grand rotation curve and the velocities shown in table 1 and figure 2 into three parts: inner part for $R \leq R_1 = 5$ kpc, which is mainly used for the bulge fitting, middle part at $1 < R \leq R_2 = 40$ kpc for the disk, and the outermost part at $1 < R \leq R_{\rm lim} = 400$ kpc for dark halo fitting. In order to fit the rapidly varying bulge component, we added the original data to the innermost fitting at $R \leq 1$ kpc.

The outermost boundary for the halo fitting was so chosen that it represents the gravitational boundary between the Galaxy and M 31, or about a half distance, 385 kpc, to M 31 at 770 kpc, as discussed in Paper II.

4.2. The Least-Squares Method

We found the best fit values of M_i and a_i for the bulge and disk by the least-squares method using the inner two parts, where the dark halo parameters are given as provisional initial values. Using the fitted bulge and disk parameters, we then found the best-fit values of ρ_0 and h for the dark halo using the outermost data. The thus-found ρ_0 and h were again used

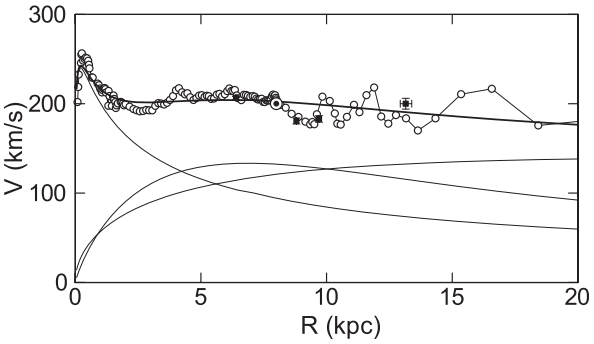

Fig. 4. Least-squares fit by the bulge, disk, and dark halo to the grand rotation curve. The thick line represents the fitted rotation curve, and the thin lines show individual contributions from bulge, disk, and halo. The observed velocities, $V(R_i)$, are shown by open circles, and the most recent accurate results from VERA (Honma et al. 2007; Oh et al. 2010) are shown by squares.

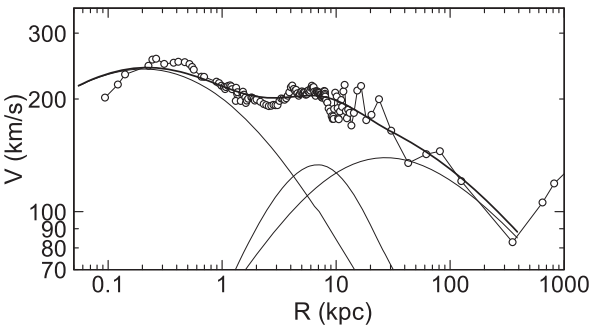

Fig. 5. Same as figure 4, but in logarithmic scaling displaying up to 1 Mpc. The dark halo was satisfactorily fitted by the NFW model. This figure demonstrates that a grand rotation curve up to $\sim$1 Mpc is essential in order to quantitatively analyze the dark halo.

in finding the disk and bulge parameters, which were further used to find the halo parameters. This procedure was repeated several times until the fitted results reached sufficiently stable values. Below, we describe the procedure in more detail.

We define ξ as

$$\xi = \sqrt{\frac{\Sigma[V_{\rm obs}(R_i) - V(R_i)]^2}{K-1}}, \tag{19}$$

where $V_{\rm obs}$ is the observed value plotted in figures 4 and 5, and K is the number of used data points in the individual data parts. Therefore, K is the number of plotted points at $R = 0$ to R_1 for the fitting of the bulge, from R_1 to R_2 for disk, and from R_2 to $R_{\rm lim}$ for the dark halo.

Here, we regard all of the plotted points to have the same weight for the following reason: since the plotted values in figure 2 are the running means of the observations, the bars in the plot are not measurement errors. Particularly, the outer data points include real velocity dispersion, while we are interested in the mean values. In order to discuss the dark halo using the outermost velocity information, it is not practical to apply such weighting that is proportional to the inverse of the square of the measurement error bars, which should give a very small weighting to the outermost rotation curve. On the other hand, in order to avoid any unnecessary smoothing of the steeply varying curve around the bulge component, the fitting was obtained by replacing the data in table 1 at $R < 1$ kpc with denser original data points before the running average.

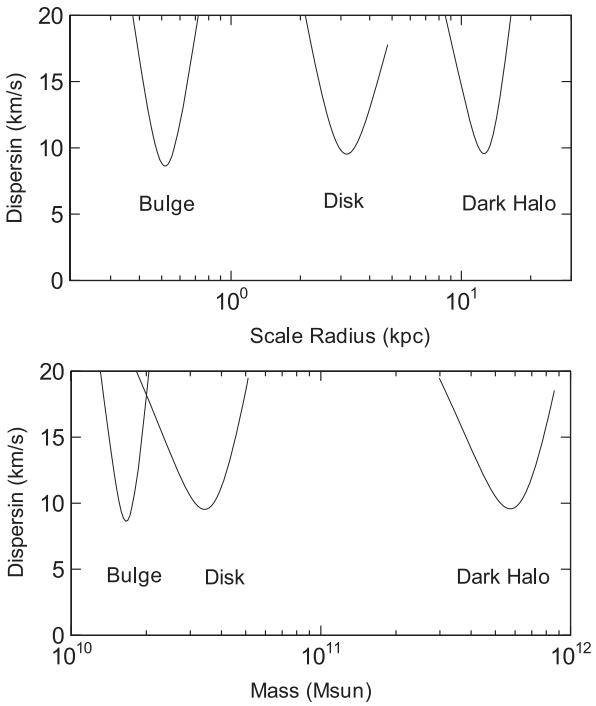

Fig. 6. (Top) Dispersion, ξ, of the fitted result as a function of each parameter ($a_{\rm b}$, $a_{\rm d}$, and h) around its best value for other parameters being fixed to the best values. (Bottom) Same as the top, but for the masses $M_{\rm b}$, $M_{\rm d}$, and $M_{\rm h}^*$.

Since the number of parameters to be determined is six ($a_{\rm b}$, $M_{\rm b}$, $a_{\rm d}$, $M_{\rm d}$, ρ_0, and h), it is not practical to obtain the best fit by one time iteration; we thus applied a step-by-step iteration as follows.

We first used the inner rotation curve, and found parameters that represent the bulge and disk components. The dark halo density was set to an arbitrary value. Thereby, we found values of $a_{\rm b}$ and $M_{\rm b}$ that minimized ξ for appropriately assumed initial values of $a_{\rm d}$ and $M_{\rm d}$. We calculated ξ by changing $a_{\rm b}$ and $M_{\rm b}$ at small steps, and fixed the best-fit values that would give minimum ξ. The thus-found $a_{\rm b}$ and $M_{\rm b}$ were used to find the best-fit $a_{\rm d}$ and $M_{\rm d}$. This procedure was repeated until the best-fit values for both the bulge and disk reached stable values. The fixed values of $a_{\rm b}$, $a_{\rm d}$, $M_{\rm b}$, and $M_{\rm d}$ were used to find the best-fit values of h and ρ_0 by the same procedure using the outer rotation curve at $1 < R \leq R_{\rm lim}$ kpc. Using the best-fit halo values, the bulge and disk fit was repeated. By repeating these procedures several times, we obatined a stable set of the six parameters.

4.3. Variations of the Fitted Parameters

Figure 6 top shows the variation of the calculated dispersion, ξ, around the best-fit value of the scale radius, $a_{\rm b}$, $a_{\rm d}$, and h as a function of each parameter with the other parameters fixed to the best values. Figure 6 bottom shows the same, but for the

Table 2. Best-fit parameters for the mass components of the Galaxy.

Mass component	Mass; Density	Scale radius	Dispersion ξ
Bulge parameters	$M_{\rm b} = (1.652 \pm 0.083) \times 10^{10}\,M_\odot$	$a_{\rm b} = 0.522 \pm 0.037\,{\rm kpc}$	$8.63\,{\rm km\,s^{-1}}$
Disk parameters	$M_{\rm d} = (3.41 \pm 0.41) \times 10^{10}\,M_\odot$	$a_{\rm d} = 3.19 \pm 0.35\,{\rm kpc}$	$9.53\,{\rm km\,s^{-1}}$
Bulge + disk mass	$M_{\rm b+d} = (5.06 \pm 0.97) \times 10^{10}\,M_\odot$		
Bulge/disk mass ratio	$M_{\rm b}/M_{\rm d} = 0.48 \pm 0.09$		
Dark halo parameters	$\rho_0 = (1.06 \pm 0.14) \times 10^{-2}\,M_\odot\,{\rm pc^{-3}}$ $= 0.403 \pm 0.051\,{\rm GeV\,cm^{-3}}$	$h = 12.53 \pm 0.88\,{\rm kpc}$	$9.57\,{\rm km\,s^{-1}}$
Local dark-matter density† at the Sun ($R = 8\,{\rm kpc}$)	$\rho_0^\odot = (6.12 \pm 0.80) \times 10^{-3}\,M_\odot\,{\rm pc^{-3}}$ $= 0.235 \pm 0.030\,{\rm GeV\,cm^{-3}}$		
Dark halo mass‡	$M_{\rm h}(R \le 8\,{\rm kpc}) = (2.71 \pm 0.42) \times 10^{10}\,M_\odot$		
	${M_{\rm h}}^*(\le h) = (5.05 \pm 0.78) \times 10^{10}\,M_\odot$	(Scaling dark halo mass)	
	$M_{\rm h}(\le 20\,{\rm kpc}) = (8.87 \pm 1.37) \times 10^{10}\,M_\odot$		
	$M_{\rm h} = M_{\rm h}(\le 385\,{\rm kpc}) = (6.52 \pm 1.01) \times 10^{11}\,M_\odot$		
Galaxy mass	$M_{\rm b+d+h} = (7.03 \pm 1.01) \times 10^{11}\,M_\odot$	($R \le 385\,{\rm kpc}$)	
Baryonic fraction	$M_{\rm b+d}/M_{\rm b+d+h} = 0.072 \pm 0.018$		

† $1\,M_\odot\,{\rm pc^{-3}} = 38.16\,{\rm GeV\,cm^{-3}}$.
‡ Error propagation included.

mass parameters. For the dark halo, the abscissa is taken as the scaling dark mass, ${M_{\rm h}}^*$.

4.4. *Error Estimates*

The errors of individual fitted parameters were evaluated as the range of the parameter that allows for an increase of the dispersion ξ by a factor of 1.1, i.e., 10% increase of the dispersion. The errors in quantities that were calculated using the fitted parameters were computed by considering the propagation through the corresponding equations.

5. The Best-Fit Galactic Parameters and Rotation Curve

Table 2 gives the best-fit parameters for the individual mass components of the Galaxy, and figures 4 and 5 show the calculated rotation curves from these parameters.

5.1. *Radii and Masses of the Bulge and Disk*

The scale radius, i.e., the half-projected-mass radius, $a_{\rm b} = 522\,{\rm pc}$, and the total mass, $M_{\rm b} = 1.652 \times 10^{10}\,M_\odot$, of the bulge are consistent with those given in the literature. The disk scale radius, $a_{\rm d} = 3.19\,{\rm kpc}$, is within the range of often quoted values, and the disk mass is $M_{\rm d} = 3.41 \times 10^{10}\,M_\odot$. The bulge-to-disk mass ratio is $M_{\rm b}/M_{\rm d} = 0.48$. This ratio is closer to that for Sbc galaxies; it is 1.0 for Sb and 0.38 for Sbc galaxies (Köeppen & Arimoto 1990).

5.2. *Dark Halo Radius and Density*

The best-fit scale radius of the dark halo was obtained to be

$$h = 12.53 \pm 0.88\,{\rm kpc}, \tag{20}$$

and the scale (representative) density

$$\rho_0 = (1.06 \pm 0.14) \times 10^{-2}\,M_\odot\,{\rm pc^{-3}} \tag{21}$$

or

$$\rho_0 = 0.403 \pm 0.051\,{\rm GeV\,cm^{-3}}, \tag{22}$$

which gives the least ξ value of

$$\xi = 9.6\ {\rm km\ s^{-1}}. \tag{23}$$

The local value near the Sun at $R = 8\,{\rm kpc}$ is estimated to be

$$\rho_0^\odot = (6.12 \pm 0.80) \times 10^{-3}\,M_\odot\,{\rm pc^{-3}}, \tag{24}$$

or

$$\rho_0^\odot = 0.235 \pm 0.030\,{\rm GeV\,cm^{-3}}. \tag{25}$$

6. Discussion

6.1. *The Grand Rotation Curve*

We have constructed the grand rotation curve of the Milky Way Galaxy using the data compiled in Paper I as well as by adding the most recent accurate measuring results. The grand rotation curve covers a wide area from the Galactic Center to the Local Group space. The curve well coincides with the circular velocity curve by Xue et al. (2008) from 7.5 to 55 kpc.

By least-squares fittings to the thus-obtained rotation curve within the boundary of the Milky Way at $R \sim 400\,{\rm kpc}$, the parameters of the three mass components (the de Vaucouleurs bulge, exponential disk, and dark halo with NFW profile) were determined at high accuracy.

The fitting was obtained more quantitatively and accurately compared to our earlier work (Papers I, II) by removing the artificial assumption of a critical radius at which the dark halo contribution becomes equal to that from the disk. The resulting fitting parameters are listed in table 2, and the fitted rotation curve is shown in figures 4 and 5.

6.2. *The Best-Fit Rotation Curve*

In the linear representation shown in figure 4, the calculated rotation curve well reproduces the observed data, except for the wavy and bumpy behaviors, which are attributable to local rings and/or arm structures, as discussed in Paper I. The fitting seems to be satisfactory almost equally in both of the two cases with and without including the dark halo. In other words, it is difficult to discuss the dark-halo problem using the current rotation curves up to $R \sim 20$–$30\,\mathrm{kpc}$.

Obviously the logarithmic expression in figure 5 makes it much easier to discriminate the dark halo contribution. A comparison of figures 4 and 5 demonstrates how the grand rotation curve is efficient, and essential to discuss the dark halo in the Milky Way. The NFW model appears to reproduce the observations sufficiently well within the data scatter.

Another interesting fact is that the most inner part at $R < 0.2\,\mathrm{kpc}$ systematically deviates from the observations: the observations more rapidly decrease toward the nucleus than the model. This indicates that the de Vaucouleurs law may not be the best expression of the innermost mass distribution.

6.3. *The Galactic Parameters*

Table 2 summarizes the obtained parameters by the present analysis, and figures 4 and 5 show the fitted rotation curves. The parameters for the bulge are not much different from those of the current work, because the corresponding rotation profile at $R \sim 1\,\mathrm{kpc}$ has a steep peak, and the least-squares fitting is more independent and effective compared to the fit to other extended components, like the disk and the halo. The total mass of the bulge and disk system, $M_{\mathrm{b+d}} = M_{\mathrm{b}} + M_{\mathrm{d}} = 5.06 \times 10^{10}\,M_\odot$, is larger than the dark mass, $M_{\mathrm{h}}(R \leq 8\,\mathrm{kpc}) \sim 2.71 \times 10^{10}\,M_\odot$, inside the solar circle. The bulge-to-disk mass ratio was found to be 0.48, which is closer to that for Sbc (0.38: Köeppen & Arimoto 1990). Our Galaxy may thus be a slightly late Sb galaxy.

We here confirm that the total mass of the bulge, disk, and dark halo within the solar circle, $M_{\mathrm{b+d}} + M_{\mathrm{h}}(R \leq 8\,\mathrm{kpc}) = 7.8 \times 10^{10}\,M_\odot \simeq M_{\mathrm{G}}$, is comparable to the simple spherical mass estimate for $V_0 = 200\,\mathrm{km\,s^{-1}}$ at $R_0 = 8\,\mathrm{kpc}$, $M_{\mathrm{G}} = R_0 V_0^2/G = 7.44 \times 10^{10}\,M_\odot$. The presently larger value is mainly due to the disk effect, and partly due to the extended bulge and disk components beyond the solar circle.

Xue et al. (2008) obtained a total mass of $(4.0 \pm 0.7) \times 10^{11}\,M_\odot$ within $R = 60\,\mathrm{kpc}$, which corresponds to $3.6 \times 10^{11}\,M_\odot$ for $V_0 = 200\,\mathrm{km\,s^{-1}}$. In our fitting result, the total mass within 60 kpc was calculated to be $(2.4 \pm 0.4) \times 10^{11}\,M_\odot$, and is consistent with their value within the error.

6.4. *NFW Dark Halo and Local Dark-Matter Density*

The NFW profile was found to fit the grand rotation curve quite well. The declining part in the outermost rotation velocity predicted by the NFW profile was clearly detected for the first time, showing a good fit to the outermost grand rotation curve at $R \sim 40$–$400\,\mathrm{kpc}$, covering the Galaxy's gravitational boundary.

The local value of the dark-matter density in the solar neighborhood, as derived from the present analysis, $\rho_0^\odot = 0.235 \pm 0.030\,\mathrm{GeV\,cm^{-3}}$, is consistent with the value of 0.2–0.4 $\mathrm{GeV\,cm^{-3}}$ by Weber and de Boer (2010). However, it is slightly smaller than the value of $0.43 \pm 0.10\,\mathrm{GeV\,cm^{-3}}$ by Salucci et al. (2010).

6.5. *Baryon Fraction*

The total Galaxy mass enclosed in the supposed gravitational boundary of the Galaxy at 385 kpc, a half distance to M 31, is $\sim 7.03 \times 10^{11}\,M_\odot$. As discussed in Paper II, this mass is not sufficient to gravitationally stabilize the Galaxy and M 31 system, and therefore the two galaxies may be embedded in a larger-scale dark-matter system properly constructing the Local Group.

If we compare the total dark-matter mass with the bulge and disk mass, we obtain an upper value to the baryon-to-dark matter ratio in the entire Galaxy shared by the bulge and disk to be

$$f_{\mathrm{bd}} = M_{\mathrm{b+d}}/M_{\mathrm{b+d+h}} \sim 0.072 \pm 0.018. \quad (26)$$

Athough this fraction is much smaller than the WMAP's cosmic value of the baryon fraction, 0.17 (Dunkley et al. 2009), it may be compared with the mean baryon fraction, $\sim$0.12, observed for groups of galaxies (Andreon 2010). If we assume that the fraction in the Galactic halo, having a radius of $\sim 385\,\mathrm{kpc}$, is the same, a small fraction, ~ 0.05 (= 0.12–0.072), corresponding to a baryon mass of $\sim 3 \times 10^{10}\,M_\odot$, may exist in the form of gas filling the dark halo at a density of $\sim 6 \times 10^{-6}\,\mathrm{cm^{-3}}$.

If the gas is diffuse H I or H_2 gas, the column density would be $N_{\mathrm{H}} \sim 7 \times 10^{18}\,\mathrm{H\,cm^{-2}}$, and the velocity width would be as wide as ~ 100–$200\,\mathrm{km\,s^{-1}}$. The brightness temperature will be $\sim 0.02\,\mathrm{K}$ for H I or $\sim 0.2\,\mathrm{mK}$ for CO (J = 1–0). Such a low brightness and diffuse line emissions are extremely difficult to be detected. Moreover, it is unlikely that such diffuse gas can remain neutral, because the internal motion is highly supersonic, and the gas is easily ionized. Alternative forms may be H I and/or H_2 clouds, but it is also unlikely that such a large amount of H I or molecular clouds, almost $\sim 10^2$-times more massive than the interstellar gas in the Galactic disk, have not been detected by the current radio surveys (e.g., Wakker & van Woerden 1997) .

One possible way for the gas to coexist in the dark halo would be that they are in the form of X-ray emitting hot plasma. The temperature would be $\sim 10^6\,\mathrm{K}$ or $\sim 1\,\mathrm{keV}$, and the electron density $n_{\mathrm{e}} \sim M_{\mathrm{bary}}/(m_{\mathrm{H}} 4\pi R^3/3) \sim 0.6 \times 10^{-5}\,\mathrm{cm^{-3}}$, corresponding to an emission measure of $\sim 10^{-5}\,\mathrm{pc\,cm^2}$ for a depth of $R \sim 385\,\mathrm{kpc}$. This emission measure is much smaller than the observed value, which is on the order of $\sim 10^{-2}\,\mathrm{pc\,cm^2}$ toward the North Galactic Pole by ROSAT (Sidher et al. 1999; McCammon et al. 2002). Hence, it is possible that the apparently "missing" baryons are in the form of hot halo gas, and are already "seen" in the ROSAT X-ray background emission, sharing its small portion.

References

Andreon, S. 2010, MNRAS, 407, 263
Begeman, K. G., Broeils A. H., & Sanders, R. H. 1991, MNRAS, 249, 523
Burkert, A. 1995, ApJ, 447, L25
de Vaucouleurs, G. 1958, ApJ, 128, 465
Dunkley, J., et al. 2009, ApJS, 180, 306
Freeman, K. C. 1970, ApJ, 160, 811
Honma, M., et al. 2007, PASJ, 59, 889
Köeppen, J., & Arimoto, N. 1990, A&A, 240, 22
McCammon, D., et al. 2002, ApJ, 576, 188
Navarro, J. F., Frenk, C. S., & White, S. D. M. 1996, ApJ, 462, 563
Salucci, P., Nesti, F., Gentile, G., & Martins, C. F. 2010, A&A, 523, A83
Sidher, S. D., Sumner, T. J., & Quenby, J. J. 1999, A&A, 344, 333
Oh, C. S., Kobayashi, H., Honma, M., Hirota, T., Sato, K., & Ueno, Y. 2010, PASJ, 62, 101
Sofue, Y. 2009, PASJ, 61, 153 (Paper II)
Sofue, Y., Honma, M., & Omodaka, T. 2009, PASJ, 61, 227 (Paper I)
Sofue, Y., & Rubin, V. 2001, ARA&A, 39, 137
Wakker, B. P., & van Woerden, H. 1997, ARA&A, 35, 217
Weber, M., & de Boer, W. 2010, A&A, 509, A25
Xue, X. X., et al. 2008, ApJ, 684, 1143